Evaluation of Proinflammatory Cytokine Pathway Inhibitors for p38 MAPK Inhibitory Potential

Rameshwar U. Kadam,[†,§] Divita Garg,[†,§] Atish T. Paul,[‡] K. K. Bhutani,[‡] and Nilanjan Roy*[,†]

Centre of Pharmacoinformatics and Department of Natural Products, National Institute of Pharmaceutical Education and Research, Sector 67, S.A.S Nagar-160 062, Punjab, India

Received June 14, 2007

The target for the anti-inflammatory natural products like amentoflavone (**2**), which act by interfering with the proinflammatory cytokine pathway (e.g., TNF-α, IL-1β, and NO synthase), is not yet well-defined. Data obtained from docking, electronic, and surface analyses shed some light on steric and electronic complementarity of these molecules to p38 MAPK, thereby suggesting a possible mechanism by which they might reduce the production of proinflammatory cytokines.

Introduction

Mitogen activated protein kinases (MAPKs) are important signal transducing enzymes that are involved in many cellular regulations. The MAPK family includes the ERK (extracellular signal-regulated kinases), JNK (c-Jun NH2-terminal kinases), and p38 MAP kinases. In recent years, a strong link has been established between p38 MAPK signaling pathway and inflammation,[1,2] resulting in buttressing of new drug development efforts for treatment of inflammation and related disorders targeting p38 MAPK. It is known that binding of tissue necrosis factor (TNF-α) and interleukin (IL-1β) to their respective receptors results in activation of signaling molecules, including p38 MAPK.[3] Upon activation, the kinase phosphorylates other downstream kinases, finally leading to the activation of nuclear factor-κB (NFκB). The activated NFκB translocates to the nucleus and binds to promoters of target genes such as that of cytokines, chemokines, COX-II, iNOS, and proteases in a sequence-specific manner and initiates their transcription. Thus, the activation of p38 MAPK cascade plays an important role in the production of proinflammatory cytokines (TNF-α, IL-1β)[1] and induction of enzymes such as COX-II and iNOS.[2,3] Pyridinylimidazoles represented by SB203580 (**1**) were the first reported class of p38 inhibitors; some of these compounds are currently under clinical trials. Some research groups have reported newer analogues that selectively inhibit p38 MAPK,[4,5] while others have focused on development of QSAR models[6,7] and docking studies[8] of synthetic p38 MAPK inhibitors.

Many compounds of natural origin belonging to polyphenol, stillbene, terpene, and alkaloid classes have also been found to be capable of interfering with TNF-α and related signaling pathways.[9] Because p38 MAPK is an important signaling molecule in this pathway, we explored p38 MAPK inhibitory potential of these new natural scaffolds using a combination of *in silico* studies that we call "validation layer approach". Using a similar approach, we had found that dual PDE4-TNFα inhibitors are capable of inhibiting *P. aeruginosa* LpxC.[10]

Material and Methods

Data Set. Forty-one anti-inflammatory natural product molecules used in this study (Figure 1, Table S1 of Supporting Information) were built using the SYBYL7.1 molecular modeling package installed on a Silicon Graphics Fuel workstation running the IRIX 6.5 operating system[11] while taking into consideration the restricted rotation and necessary configuration at chiral centers in the molecules. A systematic conformation search procedure was used to identify the lowest minima conformation that was further minimized by PM3 Hamiltonian using MOPAC. To generate accurate charge information, a single-point energy calculation was performed using AM1 Hamiltonian[12] on the PM3 geometry. Mulliken charges were assigned to all molecules.[13] A detailed account on the analysis of structural geometry of the molecules used in this study is given in Supporting Information.

Validation Layer Protocol. The general flow chart of the steps involved in validation procedure is shown in (Figure 2).

Docking Study. Docking experiments were carried out using the FlexX module in SYBYL 7.1, which considers the ligand flexibility by utilizing the incremental construction algorithm. The crystal structure of p38 MAPK in complex with inhibitor **1** was recovered from the Brookhaven Protein Data Bank (http://www.rcsb.org/pdb/) (entry code 1A9U). The active site for docking was defined with the amino acids Met109, Gly110, Leu108, Ala51, Val52, Val30, Val38, Cys39, Glu71, Lys53, Tys103, Asp168, and Arg173 falling within 7 Å radius of the cocrystallized ligand. Each docking run culminated in 30 conformationaly diverse docking modes that were scored according to FlexX scoring function. The conformation with most favorable free energy of binding (ΔG_{bind}), indicated by the highest score, was accepted as the interaction mode of the ligand.

Surface Electronic Properties Based Validation. The molecules selected from the docking study were further subjected to surface electronic properties analysis based on molecular electrostatic surface potentials, hydrogen bond acceptor/donor density, and HOMO–LUMO properties. The molecular electrostatic potentials were calculated for the AM1-MOPAC optimized geometries of selected cytokine inhibitors and superimposed onto a constant electron density (0.002 e/au^3) to provide a measure of the electrostatic potential at roughly the van der Waals surface of the molecules. The regions of positive charge were estimated as a function of the repulsion experienced by a positively charged test probe and indicate relative electron deficiency, whereas regions of negative potential were estimated as a function of the attractive force experienced by a positively charged test probe and indicate areas of electronic excess.

Hydrogen bond acceptor/donor density ($\rho_{acc/don}$) (eq 1a) for the current analysis was calculated by defining a sphere with a given cutoff radius around each surface dot and counting the number of hydrogen bond acceptors and donors on the molecular surface inside this sphere ($\rho_{nacc/don}$). This number is divided by the enclosed surface area inside the sphere (a_{total}) to get the $\rho_{acc/don}$ around the surface

* To whom correspondence should be addressed. Phone: +91 172 2214682. Fax: +91 172 2214692. E-mail: nilanjanroy@niper.ac.in.
† Centre of Pharmacoinformatics.
‡ Department of Natural Products.
§ These authors have equally contributed to the work.

10.1021/jm0706923 CCC: $37.00
Published on Web 11/08/2007

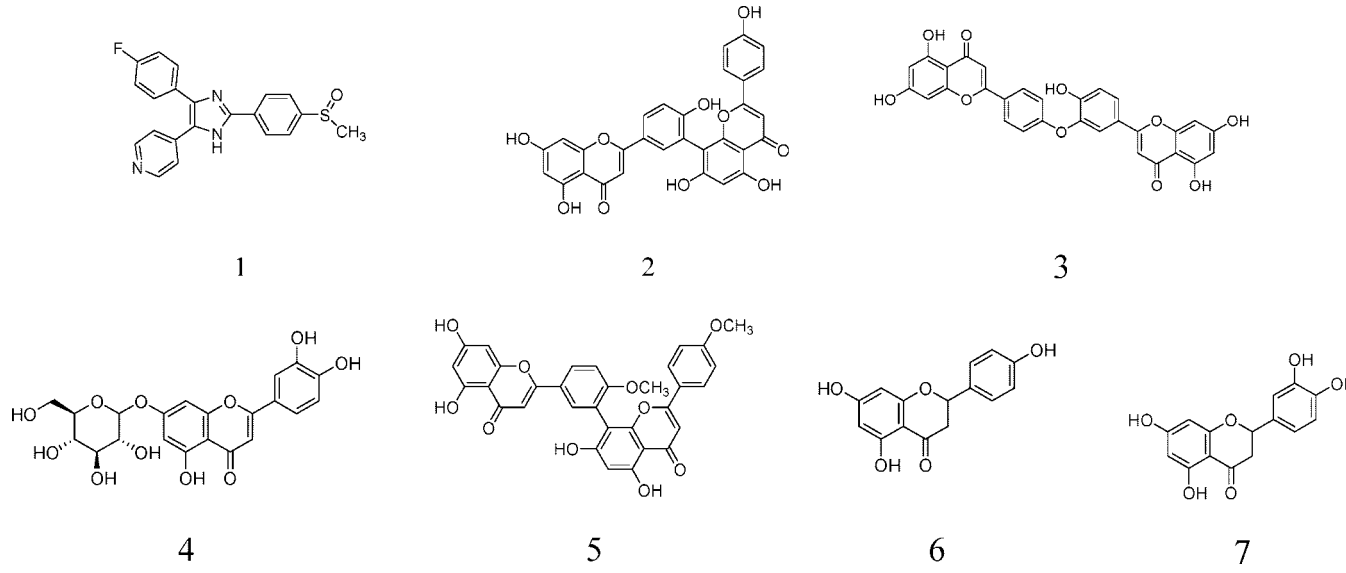

Figure 1. Structures of known p38 MAPK inhibitor (**1**) and selected cytokine inhibitor molecules **2–7**.

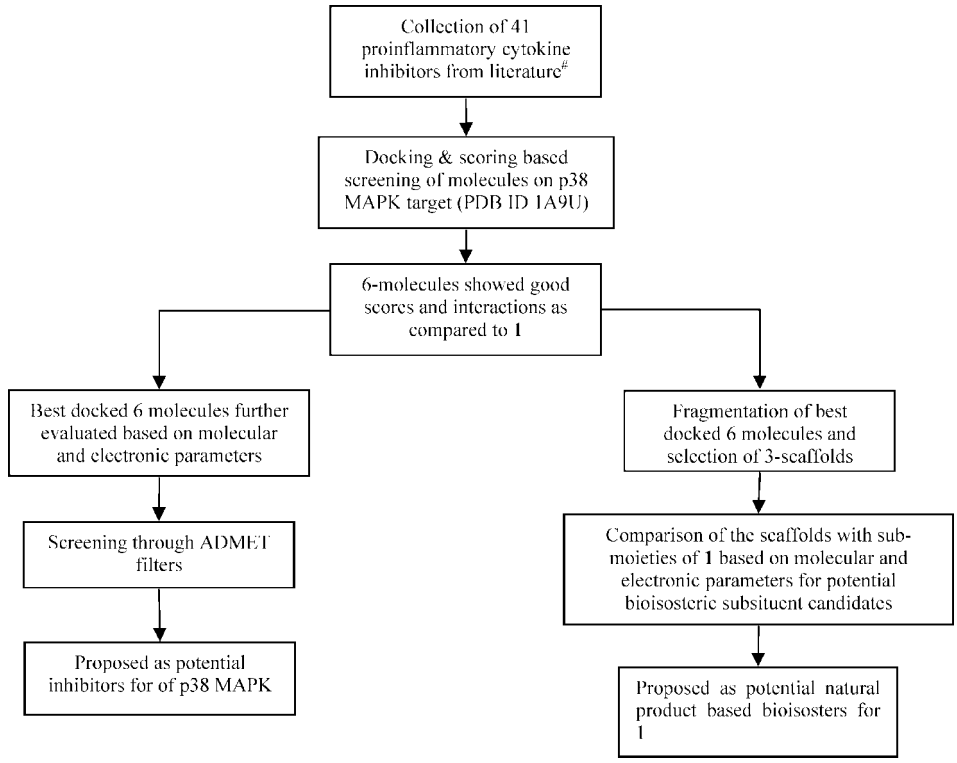

Figure 2. Flow diagram of validation layer protocol used in structure-based screening of proposed p38 MAP kinase inhibitors.# References for all collected 41 proinflammatory cytokine inhibitors from literature are given in Supporting Information.

dot in $Å^{-2}$ units. If a hydrogen donor/acceptor is inside the cutoff sphere, then $n_{acc/don} = 1$. If it is at the border of the cutoff sphere, only the surface part inside the sphere is considered, that is, $0 < n < 1$. If it is completely out of the sphere, $n_{acc/don} = 0$ (eq 1b).

$$\rho_{acc/don}(i) = \frac{\sum_j n_{acc/don}(j)}{a_{total}} \quad (1a)$$

$$n_{acc/don} = \begin{cases} 1 \\ 0 \le n \le 1 \end{cases} \quad (1b)$$

The HOMO–LUMO parameters were calculated using Cerius2 software package.

ADME/T Prediction. To select only those molecules from the screened hits that possessed drug likeness and were potentially low on toxicity, i.e., possessed a better chance of being successfully taken up as drug leads, ADME/T analysis was carried out. ADME/T studies were performed in Cerius2, version 4.10. The molecules, which were proven to be potentially druglike, were ultimately considered as potential lead molecules.

Bioisosteric Analysis. The molecules selected from the above study were fragmented to identify scaffolds that could be used to substitute the existing moieties in **1**. The new scaffolds were compared with the existing moieties based on multiple parameters, to confirm their potential as bioisosters.

Results and Discussion

The first level of our validation layer consists of docking study and analysis of docked poses to understand structural complementarity of inhibitors with p38 MAPK ligand binding site. To

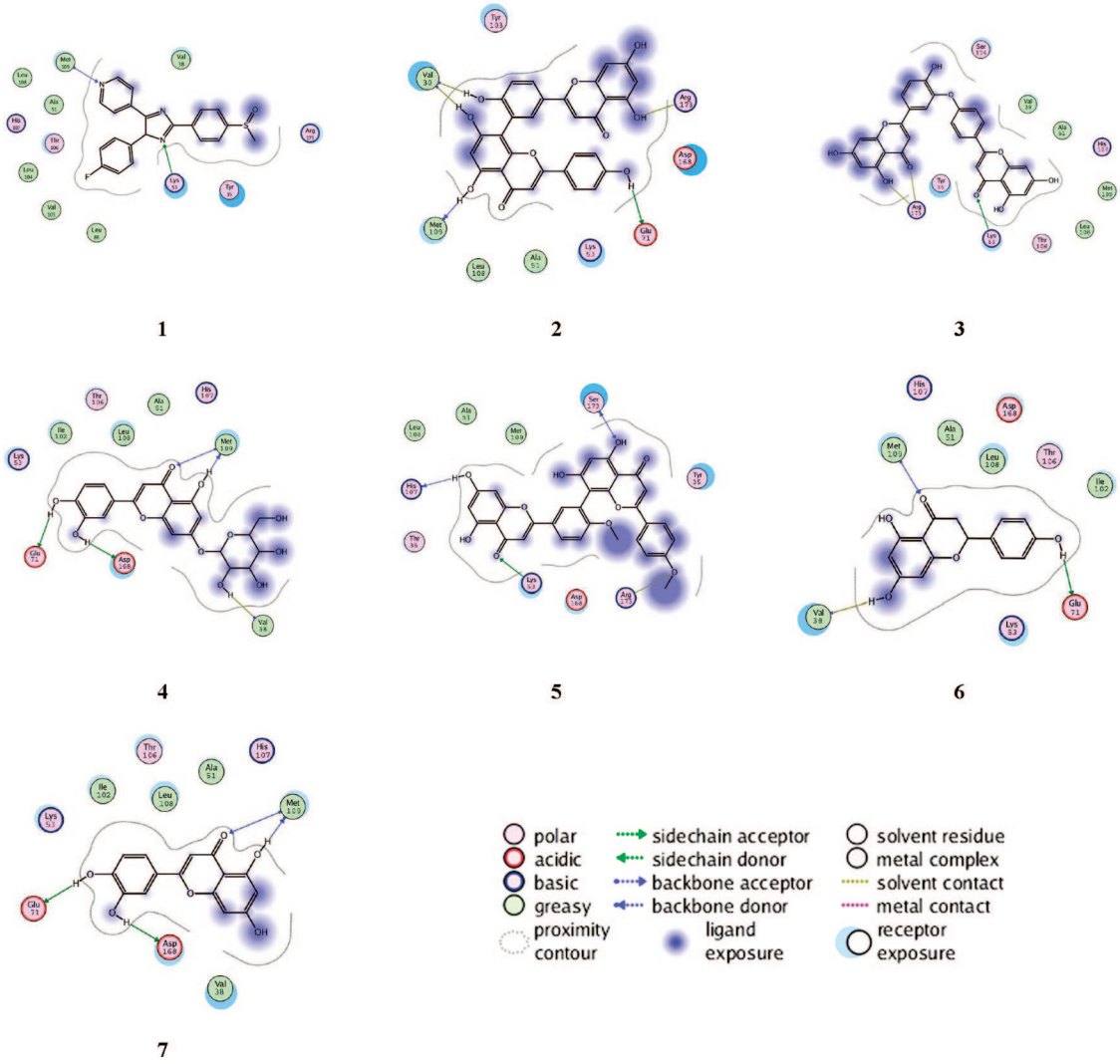

Figure 3. 2D representation of docking complex of known p38 MAPK inhibitor (**1**) and cytokine inhibitors **2–7** into p38 MAPK active site.

confirm the docking protocol, ligand **1** was extracted from the crystal structure of the cocrystallized complex 1A9U and redocked into the active site. The redocked ligand aligned in a horizontal plane similar to that presented by the bound ligand in the crystal structure with a rms value of 0.879 Å. It maintained the hydrogen bonding of the pyridine N atom of **1** with backbone amide of Met109, which forms the hinge region that connects the N and C terminal lobes of the p38 MAPK (Figure 3, **1**). This interaction is reported to be essential for ligand binding.[14] The interaction of the side chain nitrogen atom of conserved Lys53 with the N atom of the imidazole ring of **1** was also maintained. The imidazole 4-florophenyl moiety continued to interact with the hydrophobic pocket around Thr106, also called the selectivity pocket because interactions with this pocket are responsible for the selectivity of diarylimidazole inhibitors. The binding interactions defined by docked **1** were in good agreement with the published SAR data.[15–18]

Once the docking protocol was confirmed, the other molecules under analysis were docked using the same strategy. Most of the molecules docked in the same pocket as **1** but in a different plane. Amentoflavone (**2**) showed more favorable $\Delta G_{\text{binding}}$ of −26.34 kcal/mol compared to −17.95 kcal/mol for **1**. In addition to the two important interactions with Met109 and Lys53, **2** showed H-bonding interactions with Val30, Glu71, and Arg173 (Figure 3, **2**). γ-Benzopyrone ring made π-stacking interactions with Tyr35, and γ-benzopyrone 2-phenol group bound to the selectivity pocket (Figure S1, **2**). Similar interactions were observed for five other molecules. i.e., ochanoflavone (**3**), luteolin 7-glucoside (**4**), isoginketin (**5**), naringenin (**6**), and eridictyol (**7**) (Figure 3, **3**–**7**; Table 1), which showed better docking scores than **1**. Biflavones, flavones, and flavonones containing γ-benzopyrone ring showed good interactions with the backbone acceptor and donor atoms of active site residues, thereby firmly binding with the selectivity pocket. However, it was noticeable that, unlike biflavones, flavonones did not make any H-bond with Arg173 or π-stacking interactions with Tyr35. The docking scores of the other 35 cytokine pathway inhibitors, which were predicted to possess less affinity compared to the **1**, are shown in Supporting Information (Table S1).

Because the molecular recognition in ligand–receptor interactions is driven by stereoelectronic complementarity of ligands and receptors, studies of three-dimensional molecular electrostatic surface potential (MESP) and other electronic parameters have become useful for characterizing pharmacologically active molecules.[19–23] Thus, after confirming the structural complementarity of the molecules to the receptor by docking, we deemed it important to understand surface electronic properties of cytokine inhibitors to comprehend the pharmacophoric features and their complementary surface required for binding. Accordingly, the molecules selected from the docking study

Table 1. Docking Score, Number of H-Bonds and π-Stacking Interactions of Molecules **1–7** along with the Residues Involved in the Respective interactions

compd	docking score	H-bonds	residues involved	π-stackings	residues involved
2	−26.34	9	Met109, Val30, Glu71, Lys53, Arg173	1	Tyr35
3	−25.50	7	Met109, Ser 32, Lys53, Arg173	1	Tyr35
4	−20.72	7	Met109, Val30, Glu71, Lys53, Asp168	0	NA
5	−19.49	6	Met109, Val30, Hist107, Ser32, Lys53, Arg173	0	NA
6	−19.13	5	Met109, Glu71, Asp168	0	NA
7	−18.74	6	Met109, Val30, Glu68, Lys53, Asp 168	0	NA
1	−17.95	1	Met109	0	NA

Table 2. Electronic and HD Parameters

compd	most positive potential[a]	most negative potential[a]	highest HD[b]	lowest HD[b]
1	52.7	−37.20	0.02	0.000
2	43.30	−61.20	0.06	0.002
3	47.20	−59.50	0.06	0.002
4	57.60	−62.90	0.07	0.001
5	41.30	−62.00	0.06	0.001
6	45.20	−61.50	0.07	0.001
7	37.70	−47.50	0.07	0.000

[a] In kcal/mol. [b] In e/au^2.

Table 3. HOMO, LUMO, and HLG Parameters

compd	HOMO (eV)	LUMO (eV)	HLG[a] (eV)
1	−8.88	−0.64	−8.24
2	−9.08	−0.88	−8.20
3	−9.32	−1.00	−8.32
4	−9.31	−0.91	−8.40
5	−9.19	−1.00	−8.19
6	−9.27	−0.88	−8.35
7	−9.24	−0.52	−8.72

[a] HLG = HUMO-LUMO.

were analyzed on the basis of MESP, hydrogen bond donor/acceptor density (HD), and HOMO/LUMO parameters (Figures S2 and S3).

Examination of MESP of **1** (Figure S2, **A**) showed the presence of a large lateral positive potential region across the phenyl ring and a negative potential region adjacent to the nitrogen atom of the biphenyl ring. The overall positive potential on van der Waals surfaces of molecules was observed to be 40.7–52.7 kcal/mol, and the negative potential ranged from −25.2 to −37.2 kcal/mol. Analysis of the selected compounds showed that all of these structurally diverse molecules shared characteristic electronic properties among themselves and with **1** (Table 2). A negative potential of −47.50 to −62.90 kcal/mol was expressed by the carbonyl oxygen atom of γ-benzopyrone ring, which participates in electrostatic and hydrogen bonding with residues like Met109 and Val30 in the active site. The site for the most positive potential, 37.70–57.60 kcal/mol, was the hydroxyl hydrogen of γ-benzopyrone; this can facilitate interactions with the nearly polar residues in the active site. **4** (Figure S2, **D**) was an exception in which the site for the most positive potential belonged to hydrogen of glycosidic ring hydroxyl.

The HD analysis revealed further similarities between **1** and the molecules being analyzed. Like **1**, all the selected molecules showed maximum density region on the carbonyl oxygen and hydroxyl hydrogen, attached to γ-benzopyrone ring (Table 2, Figure S3).

The orbital energies of HOMO and LUMO, which are quantum chemical descriptors correlated with various biological activities, were calculated for the molecules and are reported in Table 3. Mechanistically, in ligand protein binding, the electron acceptor ability of the LUMO plays a greater role than the electron donation of the HOMO. The HOMO eigenvalues for all selected molecules were consistently more negative compared to **1**, indicating higher HOMO energies and thus firm binding of electrons to the nuclei. The LUMO eigenvalues were also more negative, indicating lower LUMO energies and stronger affinity for electrons. It was noted that the energy gap between HOMO and LUMO (HLG) for all the screened molecules was smaller (−8.32 to −8.72 eV) than the corresponding HLG values of **1** (−8.24 eV) except in the cases of **2** and **5**. The larger HLG value indicates a more stable molecule, and thus, the rearrangement of its electron density under the influence of an external electric field is harder.[24–26] Because HLG is a critical parameter determining molecular admittance, this observation supports better interactions of studied molecules than **1**. A well-defined separation in location was evidenced in the distribution of HOMO and LUMO energies, which were located in two distinct parts of the molecules. For analysis of the possible molecular interactions, HOMO and LUMO can be visualized as π-like orbitals.[27] The HOMO energy of the selected molecules lies mainly on the carbonyl oxygen part of the γ-benzopyrone ring, implying a propitiousness for strong electrostatic or π–π stacking interactions with residues of the receptor, especially Tyr35; this interaction is absent in **1**, suggesting that the presence of γ-benzopyrone ring assists in binding with p38 MAPK. On the other hand, LUMO energy was mainly located on the hydroxyl hydrogen of the γ-benzopyrone ring with a phenyl counterpart favoring the interactions with negatively charged polar residues of the receptor. These results demonstrated that the HOMO and LUMO energy distribution of the analyzed molecules is desirable for their binding with p38 MAPK.

Furthermore, to determine their suitability as drug lead candidates, the studied molecules were subjected to absorption, distribution, metabolism, excretion, and toxicity (ADME/T) analysis using Cerius2 software.[28] The data were analyzed on five criteria, which were rule of five (RO5), Cyp 2D6 inhibition, absorption level, solubility level, and hepatotoxicity (Table S2). RO5 and Cyp 2D6 inhibition are also partial indicators of absorption level and hepatotoxicity, respectively, with some additional features considered in the latter case. The molecules were predicted to be well absorbed and low on hepatotoxic potential. Moreover, because the Cyp 2D6 inhibitory potential of the molecules was predicted to be low, chances of undesirable drug interactions are less. Solubility of the molecules was predicted to be low too, which is not a desirable observation.

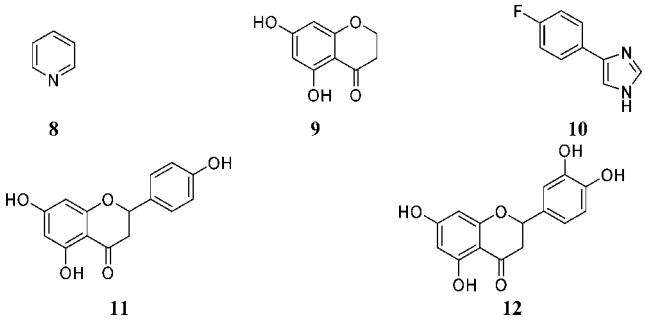

Figure 4. Structure of proposed potential natural product based bioisosters for **1**.

However, this can be improved by addition of solubilizing groups in the compound structures; such features can be used improve the ADMET profile of molecules without much altering the therapeutic profile.

From the presented investigation, it could also be hypothesized that γ-benzopyrone (**9**), γ-benzopyrone 2-phenol (**11**), and γ-benzopyrone 2-pyrocatechol (**12**) moieties (Figure 4) could be used to bioisosterically replace the imidazole 4-florophenyl moiety (**10**) of **1** while sustaining the typically conserved H-bonding pattern and other nonbonding interactions[29,30] crucial for recognition and binding to the kinase. Additionally, the replacement of pyridine (**8**) by **9** could also maintain the vital H-bonding with Met109.[31] Such efforts at modifying the known ligands have frequently been made by different groups with to separate inhibition of p38 MAPK from interference with cytochrome P450. Some of the recently reported modifications include replacement of the pyridine ring with other hydrogen bond acceptors,[32,33] introduction of sterically demanding substituents at the 2-position of the pyridine ring, introduction of substituents at the imidazole ring nitrogen adjacent to the pyridine ring,[33,34] and replacement of the imidazole ring with other five- or six- membered heterocycles.[34–37] In the design of bioisosters, it is important to consider the steric and electronic properties of the group being replaced. Knowledge of the presence or absence of hydrogen-bonding interactions is also important in the contemplation of molecular replacements.[38–40]

A computational evaluation of the above suggested natural product scaffold derived substituents, intended to replace the existing moieties in **1**, was carried out by perfoming a detailed electronic and surface analysis on them. MESP of **8** indicated that the negative potential was focused on the nitrogen, whereas in case of **9** the negative potential spread over the entire moiety with higher concentration regions on carbonyl and hydroxyl oxygens (Figure S4a). Furthermore, the carbonyl oxygen of **9** is known to have a dual acceptor potential that can aid in the H-bond contact with the NH of Met109 and neighboring residues while maintaining selectivity. Molecular dipole (μ), which is a parameter describing major contributions to long-range electrostatic interactions, was also higher for **9** (Table S3).

In addition to the electrostatics, the hydrophobic interactions with the binding site have a major contribution to the binding free energy.[41] The hydrophobic interactions at room temperature are believed to be entropy-driven because of reorganization of water molecules at the interface with the hydrophobic (nonpolar) surfaces.[42,43] The hydrophobic interaction capacity can be evaluated by the octanol–water partitioning coefficient, milogP. **9** presented a higher log *P* out of the two moieties being compared (Table S3). In terms of degree of aromaticity, **8** was closely followed by **9**. This parameter together with dispersion interactions[44] determines the strength of π–π attractions and can be evaluated by absolute chemical hardness, η, approximated by using Koopmans' theorem ($\eta = [(\text{LUMO} - \text{HOMO})]/2$).[45] Taken together, **9** seems to be more capable of interaction with the receptor compared to **8** (Table S3).

Identification of possible replacements of **10** is particularly interesting because of the presence of hydrophobic selectivity pocket in p38 MAPK. The **9**, **11**, and **12** moieties were examined as its prospective substitutes. According to docking pose analysis, these moieties bind more firmly to the selectivity pocket compared to **10**. As discussed above, the more negative MESP region is located around carbonyl and hydroxyl oxygens in γ-benzopyrone analogues (Figure S4b), whereas it is concentrated around the nitrogen in **10**. The molecular dipole (μ) for **12** was highest followed by **11**, **9**, and **10**, respectively (Table S3). The indicator of hydrophobicity, i.e., milogP hinted that moiety **11** was most hydrophobic in comparison to its counterparts. Highest aromaticity (η) was observed for the **9**, followed by **11**, **12**, and **10**, respectively (Table S3). These properties, when taken together, suggest that replacement of moiety **10** by γ-benzopyrone analogues could aid in better interactions with the hydrophobic pocket.

Conclusion

The combination of docking, electronic, and surface properties analysis and ADMET results, i.e., validation layer, enabled us to propose that one of the targets of pro-inflammatory cytokine pathway inhibitors could be p38 MAPK. The docking model predicted these molecules to have a more favorable binding to p38 MAPK than the reported inhibitor. HOMO/LUMO and surface analysis (MESP and HD) showed that the carbonyl oxygen of γ-benzopyrone ring is associated with the region where negative potential is favorable for the p38 MAPK binding, aiding in essential intercations with Met109 and Lys53. Furthermore, ADMET properties calculated are in the desirable range, so these compounds are predicted to be druglike with low toxicity potential. Thus, these molecules could be potential inhibitors of p38 MAPK and good leads for the development of newer and safer p38 MAPK inhibitors against inflammatory disorders. New scaffolds that could be used for molecular modification with the hope of improving the ligand profile were also identified.

Supporting Information Available: Geometry analysis results, docking scores, calculated parameters, and bioisosteric analysis data. This material is available free of charge via the Internet at http://pubs.acs.org.

References

(1) Lee, J. C.; Laydon, J. T.; McDonnell, P. C.; Gallagher, T. F.; Kumar, S.; Green, D.; McNulty, D.; Blumenthal, M. J.; Keys, J. R.; Land Vatter, S. W.; Strickler, J. E.; McLaughlin, M. M.; Siemens, I. R.; Fisher, S. M.; Livi, G. P.; White, J. R.; Adams, J. L.; Young, P. R. A protein kinase involved in the regulation of inflammatory cytokine biosynthesis. *Nature* **1994**, *372*, 739–745.

(2) Chen, C.; Chen, Y. H.; Lin, W. W. Involvement of p38 mitogen activated protein kinase in lipopolysaccharide-induced iNOS and COX-2 expression in J774 macrophages. *Immunology* **1999**, *97*, 124–129.

(3) Chen, C.-C.; Wang, J.-K. p38 but not p44/42 mitogen-activated protein kinase is required for nitric oxide synthase induction mediated by lipopolysaccharide in RAW 264.7 macrophages. *Mol. Pharmacol.* **1999**, *55*, 481–488.

(4) Revesz, L.; Blum, E.; Di Padova, F. E.; Buhl, T.; Fiefel, R.; Gram, H.; Hiestand, P.; Manning, U.; Rucklin, G. Novel p38 inhibitors with potent oral efficacy in several models of rheumatoid arthritis. *Bioorg. Med. Chem. Lett.* **2004**, *14*, 3595–3599.

(5) Laughlin, S. K.; Clark, M. P.; Djung, J. F.; Golebiowski, A.; Brugel, T. A.; Sabat, M.; Brookland, R. G.; Laufersweiler, M. J.; VanRens, J. C.; Townes, J. A.; De, B.; Hsieh, L. C.; Xu, S. C.; Walter, R. L.; Mekel, M. J.; Janusz, M. J. The development of new isoxazolone based inhibitors of tumor necrosis factor-α (TNF-α) production. *Bioorg. Med. Chem. Lett.* **2005**, *15*, 2399–2403.

(6) Romeiro, N. C.; Albuquerque, M. G.; de Alencastro, R. B.; Ravi, M. Construction of 4D-QSAR models for use in the design of novel p38-MAPK inhibitors. *J. Comput.-Aided Mol. Des.* **2005**, *19*, 385–400.

(7) Sperandio da Silva, G. M.; Sant'Anna, C. M. R.; Barreiro, E. J. A novel 3D-QSAR comparative molecular field analysis (CoMFA) model of imidazole and quinazolinone functionalized p38 MAP kinase inhibitors. *Bioorg. Med. Chem. Lett.* **2004**, *12*, 3159–3166.

(8) Sperandio da Silva, G. M.; Lima, L. M.; Fraga, C. A. M.; Sant'Anna, C. M. R.; Barreiro, E. J. The molecular basis for coxib inhibtion of p38α MAP kinase. *Bioorg. Med. Chem. Lett.* **2005**, *15*, 3506–3509.

(9) Paul, A. T.; Gohil, V. M.; Bhutani, K. K. Modulating TNF-α signaling with natural products. *Drug Discovery Today.* **2006**, *11*, 725–732.

(10) Kadam, R. U.; Garg, D.; Chavan, A.; Roy, N. Evaluation of *Pseudomonas aeruginosa* Deacetylase LpxC Inhibitory Activity of Dual PDE4-TNF-alpha Inhibitors: A Multiscreening Approach. *J Chem Inf Model.* **2007**, *47*, 1188–1195.

(11) *SYBYL*, version 7.1; Tripos Associates, Inc.: St. Louis, MO.

(12) Dewar, J. S.; Zoebisch, E. G.; Healy, E. F. AM1: a new general purpose quantum mechanical molecular model. *J. Am. Chem. Soc.* **1985**, *107*, 3902–3909.

(13) Mulliken, R. S. Electronic population analsys on LCAO-MO molecular wave function. *J. Chem. Phys.* **1955**, *23*, 1833–1846.

(14) Wang, Z.; Canagarajah, B. J.; Boehm, J. C.; Kassisa, S.; Cobb, M. H.; Young, P. R.; Abdel-Meguid, S.; Adams, J. L.; Goldsmith, E. J. *Structure* **1998**, *6*, 1117.

(15) Gallagher, T. F.; Fier-Thompson, S. M.; Garigipati, R. S.; Sorenson, M. E.; Smietana, J. M.; Lee, D.; Bender, P. E.; Lee, J. C.; Laydon, J. T.; Griswold, D. E.; Chabot- Fletcher, M. C.; Breton, J. J.; Adams, J. L. 2,4,5-Triarylimidazole inhibitors of IL-1 biosynthesis. *Bioorg. Med. Chem. Lett.* **1995**, *5*, 1171–1176.

(16) Boehm, J. C.; Smietana, J. M.; Sorenson, M. E.; Garigipati, R. S.; Gallagher, T. F.; Sheldrake, P. L.; Bradbeer, J.; Badger, A. M.; Laydon, J. T.; Lee, J. C.; Hillegass, L. M.; Griswold, D. E.; Breton, J. J.; Chabot-Fletcher, M. C.; Adams, J. L. 1-Substituted 4-aryl-5-pyridinylimidazoles: a new class of cytokine suppressive drugs with low 5-lipoxygenase and cyclooxygenase inhibitory potency. *J. Med. Chem.* **1996**, *39*, 3929–3937.

(17) Adams, J. L.; Boehm, J. C.; Gallagher, T. F.; Kassis, S.; Webb, E. F.; Hall, R.; Sorenson, M.; Garigipati, R.; Griswold, D. E.; Lee, J. C. Pyrimidinylimidazole inhibitors of p38: cyclic N-1 imidazole substituents enhance p38 kinase inhibition and oral activity. *Bioorg. Med. Chem. Lett.* **2001**, *11*, 2867–2870.

(18) Liverton, N. J.; Butcher, J. W.; Claiborne, C. F.; Claremon, D. A.; Libby, B. E.; Nguyen, K. T.; Pitzenberger, S. M.; Selnick, H. G.; Smith, G. R.; Tebben, A.; Vacca, J. P.; Varga, S. L.; Agarwal, L.; Dancheck, K.; Forsyth, A. J.; Fletcher, D. S.; Frantz, B.; Hanlon, W. A.; Harper, C. F.; Hofsess, S. J.; Kostura, M.; Lin, J.; Luell, S.; O'Neill, E. A.; O'Keefe, S. J. Design and synthesis of potent, selective, and orally bioavailable tetrasubstituted imidazole inhibitors of p38 mitogen-activated protein kinase. *J. Med. Chem.* **1999**, *42*, 2180–2190.

(19) Gadre, S. R.; Shirsat, R. N. *Electrostatics of Atoms and Molecules*; Universities Press: Hyderabad, India, 2000

(20) (a) Murray, J. S.; Politzer, P. The Use of Molecular Electrostatic Potential in Medicinal Chemistry. In *Quantum Medicinal Chemistry*; Wiley-VCH: New York, 2002; Vol. 17, pp 233–254. (b) Hol̈tje, H.-D.; Hol̈tje, M. Applications of Quantum Chemical Methods in Drug Design. In *Quantum Medicinal Chemistry*; Wiley-VCH: New York, 2002; Vol. 17, pp 255–274.

(21) Bhattacharrjee, A. K.; Karle, J. M. Functional correlation of molecular electronic properties with potency of synthetic carbinol-amines antimalarial agents. *Bioorg. Med. Chem.* **1998**, *6*, 1927–1933.

(22) Bhattacharrjee, A. K.; Karle, J. M. Stereoelectronic properties of antimalarial artemisinin analogues in relation to neurotoxicity. *Chem. Res. Toxicol.* **1999**, *12*, 422–428.

(23) Kadam, R. U.; Chavan, A.; Roy, N. Pharmacophoric features of *Pseudomonas aeruginosa*deacetylase LpxC inhibitors: an electronic and structural analysis. *Bioorg. Med. Chem. Lett.* **2007**, *17*, 861–868.

(24) Parr, R. G.; Pearson, R. G. Absolute hardness: companion parameter to absolute electronegativity. *J. Am. Chem. Soc.* **1983**, *105*, 7512–7516.

(25) Karelson, M.; Lobanov, V. S.; Katrinsky, A. R. Quantum-chemical descriptors in QSAR/QSPR studies. *Chem. Rev.* **1996**, *96*, 1027–1044.

(26) Pearson, R. G. Absolute electronegativity and hardness: applications to organic chemistry. *J. Org. Chem.* **1989**, *54*, 1423–1430.

(27) Cao, H.; Pan, X.-L.; Li, C.; Zhou, C.; Deng, F.-Y.; Li, T.-H. *Bioorg. Med. Chem. Lett.* **2003**, *13*, 1869–1871.

(28) *Cerius2*, version 4.10; Accelrys, Inc. (6985 Scranton Road): San Diego, CA.

(29) Mao, L.; Wang, Y.; Liu, Y.; Hu, X. Molecular determinants for ATP-binding in proteins: a data mining and quantum chemical analysis. *J. Mol. Biol.* **2004**, *336*, 787–807.

(30) Davis, A. M.; Teague, S. J. Hydrogen bonding, hydrophobic interactions, and failure of the rigid receptor hypothesis. *Angew. Chem., Int. Ed.* **1999**, *38*, 736–749.

(31) Wang, Z.; Harkins, P. C.; Ulevitch, R. J.; Han, J.; Cobb, M. H.; Goldsmith, E. J. The structure of mitogen-activated protein kinase p38 at 2.1-Å resolution. *Proc. Natl. Acad. Sci. U.S.A.* **1997**, *94*, 2327–2332.

(32) Adams, J. L.; Boehm, J. C.; Kassis, S.; Gorycki, P. D.; Webb, E. F.; Hall, R.; Sorenson, M.; Lee, J. C.; Ayrton, A.; Griswold, D. E.; Gallagher, T. F. Pyrimidinylimidazole inhibitors of CSBP/P38 kinase demonstrating decreased inhibition of hepatic cytochrome P450 enzymes. *Bioorg. Med. Chem. Lett.* **1998**, *8*, 3111–3116.

(33) Liverton, N. J.; Butcher, J. W.; Claiborne, C. F.; Claremon, D. A.; Libby, B. E.; Nguyen, K. T.; Pitzenberger, S. M.; Selnick, H. G.; Smith, G. R.; Tebben, A.; Vacca, J. P.; Varga, S. L.; Agarwal, L.; Dancheck, K.; Forsyth, A. J.; Fletcher, D. S.; Frantz, B.; Hanlon, W. A.; Harper, C. F.; Hofsess, S. J.; Kostura, M.; Lin, J.; Luell, S.; O'Neill, E. A.; O'Keefe, S. J. Design and synthesis of potent, selective, and orally bioavailable tetrasubstituted imidazole inhibitors of p38 mitogen-activated protein kinase. *J. Med. Chem.* **1999**, *42*, 2180–2190.

(34) Laufer, S. A.; Wagner, G. K.; Kotschenreuther, D. A.; Albrecht, W. Novel substituted pyridinyl imidazoles as potent anticytokine agents with low activity against hepatic cytochrome P450 enzymes. *J. Med. Chem.* **2003**, *46*, 3230–3244.

(35) Laufer, S. A.; Wagner, G. K. From imidazoles to pyrimidines: new inhibitors of cytokine release. *J. Med. Chem.* **2002**, *13*, 2733–2740.

(36) Laufer, S. A.; Margutti, S.; Fritz, M. D. Substituted isoxazoles as potent inhibitors of p38 MAP kinase. *ChemMedChem* **2006**, *1*, 197–207.

(37) Revesz, L.; Di Padova, F. E.; Buhl, T.; Feifel, R.; Gram, H.; Hiestand, P.; Manning, U.; Zimmerlin, A. G. SAR of 4-hydroxypiperidine and hydroxyalkyl substituted heterocycles as novel p38 map kinase inhibitors. *Bioorg. Med. Chem. Lett.* **2000**, *10*, 1261–1264.

(38) Langmuir, I. Isomorphism, isosterism and covalence. *J. Am. Chem. Soc.* **1919**, *41*, 1543–1559.

(39) Freidman, H. L. *Influence of Isosteric Replacement Upon Biological Activity*; National Research Council Publication No. 206; National Academy of Sciences, U.S. Government Printing Office: Washington, DC, 1951; pp 295–357.

(40) Thornber, C. W. Isosterism and molecular modification in drug design. *Chem. Soc. Rev.* **1979**, *8*, 563–580.

(41) Tsuzuki, S.; Honda, K.; Uchimaru, T.; Mikami, M.; Tanabe, K. Origin of attraction and directionality of the ð/ð interaction: model chemistry calculations of benzene dimer interaction. *J. Am. Chem. Soc.* **2002**, *124*, 104–112.

(42) De Proft, F.; Geerlings, P. Conceptual and computational DFT in the study of aromaticity. *Chem. Rev.* **2001**, *101*, 1451–1464.

(43) Davis, A. M.; Teague, S. J. Hydrogen bonding, hydrophobic interactions, and failure of the rigid receptor hypothesis. *Angew. Chem., Int. Ed.* **1999**, *38*, 736–749.

(44) Mancera, R. L.; Buckingham, A. D. Temperature effects on the hydrophobic hydration of ethane. *J. Phys. Chem.* **1995**, *99*, 14632–14640.

(45) Raschke, T. M.; Tsai, J.; Levitt, M. Quantification of the hydrophobic interaction by simulations of the aggregation of small hydrophobic solutes in water. *Proc. Natl. Acad. Sci. U.S.A.* **2001**, *98*, 5965–5969.

JM0706923